

TS-PEFT: Token-Selective Parameter-Efficient Fine-Tuning with Learnable Threshold Gating

Dabiao Ma*, Ziming Dai*, Zhimin Xin* and Shu Wang, Ye Wang, Haojun Fei

Qifu Technology, Inc.

{madabiao-jk,daiziming-jk,xinzhimin-jk,wangshu1-jk,wangye3-jk,zhangchulan-jk}@qifu.com

Abstract

In the field of large models (LMs) for natural language processing (NLP) and computer vision (CV), Parameter-Efficient Fine-Tuning (PEFT) has emerged as a resource-efficient method that modifies a limited number of parameters while keeping the pretrained weights fixed. This paper investigates the traditional PEFT approach, which applies modifications to all position indices, and questions its necessity. We introduce a new paradigm called Token-Selective PEFT (TS-PEFT), in which a function S selectively applies PEFT modifications to a subset of position indices, potentially enhancing performance on downstream tasks. Our experimental results reveal that the indiscriminate application of PEFT to all indices is not only superfluous, but may also be counterproductive. This study offers a fresh perspective on PEFT, advocating for a more targeted approach to modifications and providing a framework for future research to optimize the fine-tuning process for large models.

1 Introduction

Large models (LMs) have achieved significant progress in natural language processing (NLP) [Yao *et al.*, 2024], computer vision (CV) [Croitoru *et al.*, 2023; Liu *et al.*, 2024d], and many other fields. However, due to their large parameter scales, directly fine-tuning all parameters is often impractical in terms of computational and storage overhead. To address this issue, parameter-efficient fine-tuning (PEFT) has gradually become a mainstream paradigm for adapting pretrained large models: by freezing the base model network and introducing only a small number of trainable parameters, downstream customization can be accomplished efficiently [Hu *et al.*, 2023; Han *et al.*, 2024].

Various PEFT methods have demonstrated strong performance across a wide range of downstream tasks. Among them, prompt-based approaches (such as Prefix-Tuning [Li and Liang, 2021] and Prompt-Tuning [Lester *et al.*, 2021]) adjust model behavior by learning additional input tokens, while low-rank adaptation (LoRA) [Hu *et al.*, 2022] and its

variants (e.g., AdaLoRA [Zhang *et al.*, 2023], DoRA [Liu *et al.*, 2024c], VeRA [Kopiczko *et al.*, 2024]) update internal representations by injecting a small number of trainable parameters or low-rank components into the base model. These approaches significantly reduce the number of trainable parameters while typically maintaining performance comparable to, or even approaching, full-parameter fine-tuning.

Most existing PEFT methods, however, implicitly rely on a key assumption: once a layer is selected as the target module for PEFT, all token positions passing through this module should receive a trainable modification. Formally, for an input sequence $X = \{x_i\}_{i=1}^T$ and a frozen weight matrix W_0 , the hidden state at position i is typically written as:

$$h_i = W_0 x_i + M(x_i), \quad (1)$$

where $M(\cdot)$ is a PEFT module such as LoRA. This “update-all-positions” design ignores the fact that different token positions contribute unequally to the downstream objective.

In practice, we observe that, for already strong pretrained models, the deviation induced by PEFT is extremely small on many token positions, while only a small subset of positions exhibit substantial and task-relevant changes. In other words, most PEFT updates are effectively redundant at the token level. Uniformly applying modifications to all positions not only injects unnecessary noise and potential interference, but also increases computation, especially when multiple PEFT modules are stacked. This motivates a natural question: **can PEFT be made selective over token positions instead of blindly updating every one of them?**

Our empirical findings suggest a negative answer. We propose a simple yet effective framework, **Token-Selective PEFT (TS-PEFT)**, which enables token-level selective parameter-efficient fine-tuning. Instead of always applying $M(x_i)$ to every position, TS-PEFT introduces a binary gating function S at each token position that decides whether to add the PEFT update or to keep the base model output unchanged. Intuitively, positions whose PEFT updates are small relative to the frozen output remain untouched, while positions with larger, more impactful updates retain their PEFT modifications, yielding a token-level sparse pattern of PEFT updates.

In the experimental section, we conduct systematic evaluations on representative models including LLaMA-3-8B, LLaVA-1.5-7B, and DeBERTaV3-base [He *et al.*, 2021], covering commonsense reasoning, visual instruction tuning,

*Equal contribution.

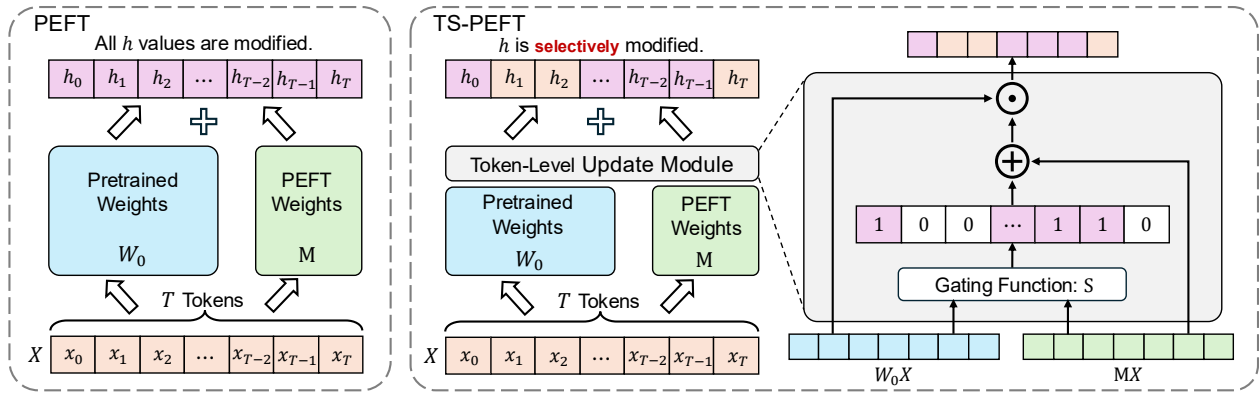


Figure 1: Comparison between standard PEFT and our TS-PEFT framework.

and natural language understanding. The results show that, on top of strong PEFT baselines such as LoRA, DoRA, AdaLoRA, and Adapter, TS-PEFT consistently matches or surpasses their performance while applying updates to only about 40–60% of token positions. Moreover, the learned token-level sparsity patterns can be aggregated into module-level importance indicators, which enable selecting fewer yet more critical tuning modules that even outperform full-module fine-tuning under comparable parameter budgets. In summary, our contributions are as follows:

- We point out and examine a neglected aspect of standard PEFT: once a layer is chosen as a target module, all token positions are updated uniformly, even though only a small fraction of positions contribute meaningfully to the downstream objective. Our empirical analysis of token-level sparsity shows that many PEFT updates induce negligible deviation from the frozen backbone, revealing substantial redundancy along the sequence dimension and motivating selective updates.
- We propose TS-PEFT, which introduces a token-level binary gating function on top of existing PEFT modules. By formulating the learning of layer-wise thresholds as a sparsity-regularized proximal optimization problem, deriving a practical approximate gradient, and applying Adam-style moment estimation, TS-PEFT enables stable end-to-end training of token-level gates jointly with PEFT parameters. The framework is agnostic to the specific low-rank parameterization and can be used as a plug-in module for a variety of PEFT methods.
- On three representative benchmarks, TS-PEFT consistently matches or surpasses strong PEFT baselines, while updating only 40%-60% token positions. Moreover, the learned token-level sparsity patterns can be aggregated into module-wise importance scores, enabling selective tuning of fewer but more critical modules that can outperform full-module fine-tuning under comparable parameter budgets.

2 Related Work

Low-Rank Adaptation. Low-rank adaptation and its derivatives have demonstrated strong potential in reducing the num-

ber of trainable parameters while preserving downstream performance. LoRA [Hu *et al.*, 2022] introduces two low-rank trainable matrices A and B to approximate weight updates, thereby avoiding direct modification of full weight matrices in large pretrained models; after training, these matrices can be merged back into the base model without incurring additional inference cost. Building on this idea, AdaLoRA [Zhang *et al.*, 2023] adaptively redistributes the effective rank across different layers to better meet task-specific requirements, DoRA [Liu *et al.*, 2024c] refines the decomposition of weight updates to improve the expressiveness and stability of low-rank adaptation, and VeRA [Kopitzko *et al.*, 2024] leverages shared low-rank bases to further reduce per-task parameter overhead. However, all these methods implicitly assume that once a layer is selected as the PEFT target, every token position passing through that layer should receive an update—that is, they perform parameter compression at the module level while still maintaining dense updates along the positional dimension. This may introduce unnecessary redundant modifications and fails to explicitly characterize or exploit potential token-level redundancy.

Sparsity. Sparsity-guided methods have been widely used to improve the efficiency and interpretability of large language models. By reducing the number of active parameters and concentrating computation on core components, these approaches not only make models more efficient but also offer clearer insights into their decision-making processes. Mixture-of-experts (MoE) models, exemplified by Switch Transformers [Fedus *et al.*, 2022] and Mixtral 8x7B [Jiang *et al.*, 2024], employ sparse activation to keep the computational cost roughly constant even with a very large number of parameters, and several recent works have combined MoE architectures with LoRA-style adapters to further enhance performance [Chen *et al.*, 2024; Liu *et al.*, 2024b; Zadouri *et al.*, 2024]. Another typical use of sparsity is model pruning, where less influential parameters are removed while preserving important ones to maintain accuracy under lower computational budgets [Ma *et al.*, 2023; Xu *et al.*, 2024; Xia *et al.*, 2024]. [Tan *et al.*, 2024] further introduce sparsity-guided techniques as a tool for interpreting the behavior of LLMs. However, most existing studies focus on parameter-wise sparsity, i.e., deciding which weights or

modules to activate or prune. In contrast, our work explores token-level sparsity in the context of PEFT: instead of sparsifying parameters, we selectively decide which token positions should receive PEFT updates, revealing and leveraging redundancy along the sequence dimension.

3 Method

This section presents the overall theoretical framework and optimization process of TS-PEFT. We first formalize the LoRA-style PEFT procedure and introduce a token-level control function S to determine whether a PEFT update should be applied at each position. Then, we formulate the learning of the scalar threshold τ in S as an optimization problem with a sparsity regularization term. Next, to address the non-differentiability of S with respect to τ and the issue that gradients are nearly zero at most positions, we derive a computable approximate gradient. Finally, we combine this approximate gradient with momentum and adaptive learning-rate mechanisms so that it can be seamlessly integrated into the Adam optimizer, and we provide the overall algorithmic description of the TS-PEFT training process.

3.1 Token-level Selective PEFT Formulation

As shown in Eq.(1), once a layer is selected as a PEFT target layer, all token positions passing through that layer will uniformly receive the increment introduced by $M(x_i)$. To break this assumption, we introduce a token-level gating function S on top of Eq.(1) to determine whether a PEFT update is actually applied at each position. Specifically, the output h_i at position i is rewritten as:

$$h_i = \begin{cases} W_0 x_i & \text{if } S(W_0 x_i, M(x_i)) = 0, \\ W_0 x_i + M(x_i) & \text{if } S(W_0 x_i, M(x_i)) = 1. \end{cases} \quad (2)$$

Here, $S(\cdot) \in \{0, 1\}$ serves as a gating variable: when $S = 1$, the update is enabled at that position, and when $S = 0$, the position retains the base model output. To instantiate Eq.(2), we focus on the relative magnitude r_i of the PEFT update with respect to the base model output at each position i : $r_i = \|M(x_i)\|_2 / \|W_0 x_i\|_2$. This is because the feature norm values at different layers vary significantly. The relative values enable each layer to adaptively adjust according to its own weight change ratio. Intuitively, a larger r_i means that the PEFT update induces a stronger perturbation relative to the base model output at that position and is more likely to be task-relevant, whereas a small r_i indicates that the modification is minor and can be treated as negligible. Therefore, we introduce a learnable scalar threshold τ for each target layer and define the control function accordingly:

$$S(W_0, M(x_i)) = \begin{cases} 0 & \text{if } r_i < \tau, \\ 1 & \text{if } r_i \geq \tau. \end{cases} \quad (3)$$

In other words, when the relative magnitude at a given position is not lower than τ , we consider the update at that position worth retaining; otherwise, the update for that position is skipped. This results in a token-level sparse update pattern along the sequence dimension within each selected PEFT module, with the threshold τ directly controlling the overall sparsity level.

However, this threshold-based step gating introduces two training challenges: first, S is a non-smooth step function with respect to τ , so standard backpropagation provides almost no useful gradients; second, we want S to activate PEFT updates only on a subset of token positions while keeping the remaining ones identical to the backbone, which requires explicit control of the overall sparsity level during threshold learning. The next subsections tackle these two issues via a proximal objective and a computable gradient approximation.

3.2 Proximal Optimization for the Threshold

Due to the training difficulties mentioned above, directly using first-order optimization methods cannot effectively update τ . Therefore, to ensure that the threshold can be stably updated during training, we formulate its learning process as a proximal optimization problem, allowing it to follow the changes in the original task loss while explicitly favoring a sparser update pattern. Specifically, our objective function is defined as follows:

$$\min \mathcal{L}(\tau) = \ell(\tau) + \lambda \sum_i \mathbb{1}(r_i \geq \tau), \quad (4)$$

where $\ell(\tau)$ denotes the loss of the target task, and the second term penalizes the number of excessively activated tokens to encourage a sparser update, $\mathbb{1}(\cdot)$ is the indicator function, and λ serves as a hyperparameter that balances the sparsity level.

However, since the indicator function is non-differentiable, we adopt proximal optimization techniques and introduce a quadratic regularization term in the threshold update to limit its fluctuation [Parikh *et al.*, 2014]. Given the threshold τ^k at the k -th iteration, the update τ^{k+1} can be written as:

$$\operatorname{argmin}_\tau \left[\ell(\tau) + \frac{\partial \ell}{\partial \tau}(\tau - \tau^k) + \frac{1}{2\alpha_k} |\tau - \tau^k|^2 + \lambda P(\tau) \right], \quad (5)$$

where α_k is the step size. For convenience in the subsequent derivation, we set $\sum_i \mathbb{1}(r_i \geq \tau)$ to be $P(\tau)$. It can be seen that this subproblem consists of three components: a first-order approximation of the loss at τ^k , a proximal term that constrains the magnitude of the update, and a sparsity regularization term that favors fewer activated positions.

To solve Eq.(5), we need to compute $\partial \ell / \partial \tau$ and $\partial P / \partial \tau$. Thus, we first expand the output in Eq.(2) along the hidden dimension. Let the hidden representation of the i -th token at dimension $j \in \{0, \dots, H-1\}$ be denoted as:

$$h_{ij} = [W_0 x_i]_j + [M(x_i)]_j * \mathbb{1}(r_i \geq \tau), \quad (6)$$

where H is the hidden size, and $[\cdot]_j$ denotes the j -th component of a vector. By backpropagation, we finally get:

$$\frac{\partial \ell}{\partial \tau} = \sum_i \mu_i \frac{\partial}{\partial \tau} \mathbb{1}(r_i \geq \tau), \quad (7)$$

$$\frac{\partial P}{\partial \tau} = \sum_i \lambda \frac{\partial}{\partial \tau} \mathbb{1}(r_i \geq \tau), \quad (8)$$

where μ_i aggregates the overall influence of the PEFT update at position i on the loss:

$$\mu_i = \sum_{j=0}^{H-1} \frac{\partial \ell}{\partial h_{ij}} [M(x_i)]_j. \quad (9)$$

Algorithm 1 Forward and Backward

- 1: **Input:** $M, \alpha_k, s, \lambda, \beta_1, \beta_2, \tau^k$.
- 2: **Output:** τ^{k+1} , updated parameters of M .
- 3: **Forward Pass:**
- 4: Forward as in Eq.(2).
- 5: **Backward Pass:**
- 6: **Step 1:** Perform the usual backward step to update parameters of M .
- 7: **Step 2:**
- 8: Compute μ_i as in Eq.(9).
- 9: Compute g_k as in Eq.(15).
- 10: Update τ^{k+1} as in Eq.(20).

3.3 Gradient Approximation for the Step Function

In the previous subsection, we obtained the derivative expressions of the loss function and the sparsity penalty term with respect to the threshold τ . However, all these derivatives depend on the partial derivative of the step gating $\mathbb{1}(r_i \geq \tau)$ with respect to τ , whose numerical value is almost zero everywhere, making it impossible to directly perform gradient updates. Therefore, to enable stable learning of the threshold through backpropagation, this section constructs a computable gradient approximation (based on the perspective of proximal optimization) to replace the non-differentiable derivative of the indicator function.

A straightforward approximation is to treat the gradient of the step function as a constant $-s, s > 0$, that is:

$$\frac{\partial}{\partial \tau} \mathbb{1}(r_i \geq \tau) \approx -s. \quad (10)$$

Substituting this approximation into Eq.(7)-(9) yields the “rough” gradients of the loss term and the sparsity term with respect to the threshold:

$$\frac{\partial \ell}{\partial \tau} \approx -s \sum_i \mu_i, \quad (11)$$

$$\frac{\partial P}{\partial \tau} \approx -s \sum_i \lambda. \quad (12)$$

However, we observe that Eq.(12) will always push τ upward, while the direction of Eq.(11) depends on the sign of μ_i , making Eq.(10) a rather coarse approximation. To avoid unstable oscillation, we further introduce a consistency mask so that only tokens whose PEFT updates “should be activated” contribute to the threshold update. Concretely, we only use positions where the current gating decision agrees with their importance estimate ($\mathbb{1}(\mu_i \geq 0) = \mathbb{1}(r_i \geq \tau)$). Therefore, we revise Eq.(11) and Eq.(12) as follows:

$$\frac{\partial \ell}{\partial \tau} = -s \sum_i \mathbb{1}[\mathbb{1}(\mu_i \geq 0) = \mathbb{1}(r_i \geq \tau)] \mu_i, \quad (13)$$

$$\frac{\partial P}{\partial \tau} = -s \sum_i \mathbb{1}(r_i \geq \tau) \lambda. \quad (14)$$

The constraints can be interpreted as follows: whenever τ is either large enough ($\mu_i \geq 0, r_i < \tau$) or small enough ($\mu_i \leq 0, r_i \geq \tau$) to render the update of τ unnecessary, Eq.(13) zeros

$\partial \ell / \partial \tau$; similarly, when τ is large enough ($r_i < \tau, \lambda$ is a positive constant), Eq.(14) nullifies $\partial P / \partial \tau$.

Combining both parts, the approximate gradient for updating the threshold can be unified as:

$$g_k = \sum_i \{\mathbb{1}[\mathbb{1}(\mu_i \geq 0) = \mathbb{1}(r_i \geq \tau)] \mu_i + \mathbb{1}(r_i \geq \tau) \lambda\}. \quad (15)$$

Finally, given the learning rate α_k , the threshold is updated as $\tau^{k+1} = \tau^k + \alpha_k s \cdot g_k$, where $-\alpha_k s$ can be regarded as the learning rate.

3.4 Adam-style Threshold Update and Overall Training Procedure

In practice, the approximate gradient g_k for the threshold τ is highly noisy and varies in scale across training steps: the contributions of tokens change significantly between batches, and the magnitude of g_k can fluctuate during optimization. Directly applying plain gradient descent to τ therefore tends to cause oscillation and slow or unstable convergence. To mitigate this, we update each threshold with an Adam-style rule that combines momentum and adaptive learning rates[Kingma *et al.*, 2015].

At the k -th iteration, we use the approximate gradient g_k obtained in the previous subsection to update the first and second moments:

$$m_k \leftarrow \beta_1 m_{k-1} + (1 - \beta_1) g_k, \quad (16)$$

$$v_k \leftarrow \beta_2 v_{k-1} + (1 - \beta_2) g_k^2, \quad (17)$$

$$\hat{m}_k \leftarrow m_k / (1 - \beta_1^k), \quad (18)$$

$$\hat{v}_k \leftarrow v_k / (1 - \beta_2^k), \quad (19)$$

where β_1 controls the contribution of past gradients and β_2 governs the decay rate of squared gradients, while \hat{m}_k and \hat{v}_k denote the bias-corrected first- and second-moment estimates used in the Adam update. Finally, the threshold is updated as:

$$\tau^{k+1} \leftarrow \tau^k + \alpha_k s \frac{\hat{m}_k}{\sqrt{\hat{v}_k} + \epsilon}, \text{ with } \tau^0 = 0. \quad (20)$$

where s is the gradient scaling factor, and ϵ prevents division by zero. In practice, this Adam-style update yields stable convergence of the thresholds under noisy gradients while preserving the desired sparsity level.

Combining the above components, the training process of TS-PEFT can be summarized as follows: in each training step, during the forward pass, we perform gating based on each token’s relative update magnitude r_i and the threshold τ of the corresponding layer, applying updates only at positions that satisfy the condition while keeping the backbone output unchanged at all other positions. Then, standard backpropagation is used to update all PEFT parameters, while the backbone parameters remain frozen throughout. On this basis, we compute μ_i to construct the approximate gradient g_k for the threshold, and independently update the threshold τ of each layer using Adam-style first- and second-moment estimates. The full training procedure is presented in Algorithm 1.

	<i>Hyperparams</i>	PIQA	BoolQ	HellaSwag	WinoGrande	SIQA	OBQA	ARC-e	ARC-c	Avg
LoRA	$s = 4e-5$	88.5	64.2	95.3	85.5	80.8	85.4	90.3	79.9	83.7
TS-LoRA	$\lambda = 4.5e-5$	88.6	70.1	95.5	84.4	82.3	85.8	90.1	79.4	84.5
Sparsity(%)		58.8	55.6	57.1	54.0	54.9	56.8	59.2	60.0	57.1
DoRA	$s = 4e-5$	87.5	75.0	95.5	85.5	80.1	85.8	90.8	79.5	85.0
TS-DoRA	$\lambda = 1e-5$	88.8	75.2	95.5	87.1	80.2	86.6	91.2	80.1	85.6
Sparsity(%)		50.0	47.9	50.2	47.1	47.6	48.3	49.6	50.0	48.8
AdaLoRA	$s = 4e-5$	88.8	74.2	95.5	85.2	79.6	85.4	91.2	79.5	84.9
TS-AdaLoRA	$\lambda = 1e-4$	88.4	75.5	95.8	85.6	80.9	86.2	90.1	79.9	85.3
Sparsity(%)		74.3	76.0	65.0	70.8	68.9	72.8	75.5	75.9	67.7

Table 1: Evaluation scores of LLaMA3.1-8B on CSR benchmarks; the last row in each block shows the sparsity of TS-PEFT.

4 Experiments

4.1 Experimental Setup

We evaluate TS-PEFT across three representative scenarios: natural language understanding (NLU), commonsense reasoning (CSR), and visual instruction tuning (VIT). The experimental setup covers the datasets, baseline models, and hyperparameter configurations to ensure reproducibility and comparability of the results.

Datasets and Models. We select several representative benchmarks in the current PEFT and small-model fine-tuning literature. For CSR, we evaluate on LLaMA-3.1-8B [Dubey *et al.*, 2024] using PIQA, BoolQ, HellaSwag, WinoGrande, SIQA, OBQA, and ARC-e/ARC-c, covering typical language reasoning scenarios such as physical commonsense, Boolean question answering, narrative completion, and scientific QA [Liu *et al.*, 2024c]. For VIT, we evaluate LLaVA-1.5-7B [Liu *et al.*, 2023; Liu *et al.*, 2024a] on ScienceQA, POPE, MMBench, GQA, VisWiz, VQAv2, and VQAT, which are generative language tasks with open-ended answers conditioned on images and textual instructions, rather than fixed-choice classification. For NLU, we build on DeBERTaV3-base [He *et al.*, 2021] and use the GLUE benchmark datasets [Wang *et al.*, 2018]. The GLUE tasks follow the official evaluation protocol: CoLA uses the Matthews correlation coefficient, STS-B uses correlation coefficients, and all other tasks use accuracy.

Baselines. In our experiments, we select several mainstream parameter-efficient fine-tuning methods as baselines, covering two major categories: low-rank update methods and adapter-based methods. Specifically, LoRA, DoRA, and AdaLoRA are used to examine whether TS-PEFT can consistently provide additional gains under different low-rank update strategies, while Parallel Adapter [Hu *et al.*, 2023] is included to evaluate the method’s scalability on adapter-style architectures. For each baseline, we keep its original implementation, hyperparameters, and rank configuration unchanged, and apply TS-PEFT on top of it. This ensures that the comparison is not affected by factors unrelated to the baseline itself and that the results accurately reflect the impact of token-level selective updates.

Training details. In all experiments, we freeze the backbone model and update only the PEFT parameters and the

threshold τ . We use the AdamW optimizer, where the PEFT parameters and τ share the same base learning rate, while the effective learning rate of τ is further modulated by the scaling factor s . For text tasks, we follow standard instruction-tuning configurations; for vision-language tasks, we adopt the original training pipeline of the corresponding models. Unless otherwise specified, we set $\alpha_k = 1$, $\beta_1 = 0.9$, and $\beta_2 = 0.98$. Each main experiment is repeated at least three times with different random seeds, and we report the mean scores across runs. Additional hyperparameter settings are summarized in Appendix A.4.

4.2 Experimental Results

Commonsense Reasoning. Table 1 reports the results of various PEFT methods and their TS-PEFT variants on the CSR tasks. For a fair comparison, we set the rank of both LoRA and DoRA to 32, and configure AdaLoRA with an initial rank of 64 and a target rank of 32. Under the same rank settings, we observe that TS-LoRA, TS-DoRA, and TS-AdaLoRA achieve performance comparable to or better than their respective baselines on most datasets. This indicates that selectively skipping updates on a subset of tokens does not weaken downstream performance; instead, it can help mitigate the interference caused by redundant updates.

The table also reports the sparsity rate of TS-PEFT (i.e., the proportion of positions in the input sequence that are not modified by the PEFT output, as defined in Eq.(21)). Across different baselines and tasks, this proportion remains roughly within the 40%–60% range, meaning that fewer than half of the tokens actually receive PEFT updates. Even under this degree of sparsity, TS-PEFT is able to match or outperform the original baselines in commonsense reasoning, suggesting that standard PEFT exhibits substantial redundancy along the token dimension, and that threshold-based token-level selective updating provides a more efficient use of PEFT capacity.

$$\text{Sparsity}(W_0, M, X) = 1 - \frac{1}{T} \sum_i S(W_0 x_i, M(x_i)). \quad (21)$$

Visual Instruction Tuning. For visual instruction tuning, we follow the training setup of [Liu *et al.*, 2024c], configuring LoRA and DoRA with rank 128 and setting the initial and target ranks of AdaLoRA to 256 and 128. Table 2 shows the results. Across all benchmarks, TS-LoRA, TS-DoRA,

	<i>Hyperparams</i>	SQA	POPE	MMBench	GQA	VisWiz	VQAv2	VQAT	Avg
LoRA		68.1	87.3	64.8	63.1	46.8	79.1	57.3	66.6
TS-LoRA	$s = 4e-5$ $\lambda = 2e-6$	68.3	87.5	63.6	63.3	50.4	78.3	57.5	67.0
Sparsity(%)		67.6	59.3	62.0	59.3	59.5	59.2	62.2	61.3
DoRA		67.5	87.4	65.5	63.0	50.5	78.6	57.0	67.1
TS-DoRA	$s = 4e-5$ $\lambda = 1e-6$	69.4	88.0	64.7	62.4	54.2	77.8	55.9	67.4
Sparsity(%)		70.6	62.6	65.2	62.4	62.9	63.8	65.2	64.7
AdaLoRA		68.0	87.3	64.3	61.7	48.9	78.3	56.9	66.5
TS-AdaLoRA	$s = 4e-5$ $\lambda = 5e-7$	67.8	87.5	63.4	62.3	52.6	78.5	55.2	66.8
Sparsity(%)		60.0	50.9	54.1	50.9	51.4	50.9	53.9	53.2

Table 2: Evaluation scores of LLaVA-1.5-7B on VIT benchmarks; the last row in each block shows the sparsity of TS-PEFT.

Method	MNLI	CoLA	QNLI	RTE	MRPC	QQP	SST-2	STS-B	Avg
LoRA	89.9	69.2	94.1	87.1	90.4	92.2	95.3	91.8	88.8
TS-LoRA	89.9	70.3	94.2	88.1	91.2	92.0	95.8	91.5	89.1
Sparsity(%)	71.6	64.1	70.6	42.8	55.4	57.1	67.6	33.9	57.9
λ	1e-5	6e-6	2e-5	1e-5	1e-5	2e-6	2e-5	8e-5	-
AdaLoRA	90.4	71.1	94.6	88.6	91.3	91.9	95.9	91.9	89.5
TS-AdaLoRA	90.5	71.3	94.5	89.0	91.6	91.9	96.1	91.6	89.6
Sparsity(%)	55.2	53.1	68.1	62.7	71.7	54.7	56.9	68.3	61.3
λ	9e-6	5e-6	4.5e-7	2e-6	2e-8	5e-7	2e-6	5e-6	-
Adapter	90.4	72.1	94.2	86.6	90.0	92.1	95.6	91.4	89.1
TS-Adapter	90.1	72.0	94.1	86.8	91.4	91.8	96.6	91.3	89.3
Sparsity(%)	56.4	59.4	65.5	62.7	55.1	58.0	56.2	67.7	60.1
λ	5e-7	4.5e-7	4.5e-7	2e-6	2e-8	5e-7	2e-6	5e-6	-

Table 3: Evaluation scores of DeBERTaV3-base on GLUE benchmarks; the “Sparsity(%)” rows show the sparsity of TS-PEFT, and the “ λ ” rows list task-wise thresholds ($s = 1e-4$).

and TS-AdaLoRA yield consistent improvements of about 0.3–0.4 points, while operating under 50–65% token sparsity. This demonstrates that token-level redundancy is also present in multimodal generative tasks, and selective token updates remain effective, consistent with our observations in CSR.

Natural Language Understanding. The results are shown in Table 3, where the target ranks of LoRA and AdaLoRA are both set to 4. Overall, TS-LoRA and TS-AdaLoRA achieve average performance that is comparable to or slightly better than their respective baselines, consistent with the trends observed in the previous two task categories. To test whether our approach is tied to a specific low-rank parameterization, we further include Parallel Adapter as a non-LoRA-style PEFT baseline and apply TS-PEFT on top of it to obtain TS-Adapter, using a hidden size of 32. The results show that TS-Adapter performs no worse than the original Adapter, suggesting that TS-PEFT is not bound to LoRA-style weight structures, but can function as a general token-level gating layer that can be stacked on diverse PEFT modules.

TS-PEFT introduces token-level sparsity as a logical mask. Therefore, the current implementation does not provide wall-clock speedups. However, the theoretical computation reduction is significant. With specialized kernels support for sparse matrix additions in the future, TS-PEFT has the potential to

translate this logical sparsity into physical latency reduction.

4.3 In-depth Analysis

Necessity of Adaptive Moment Estimation. To verify the effect of the adaptive momentum estimation module, we conduct ablation experiments by removing this component. In this case, the threshold τ exhibits noticeable oscillation and gradually diverges, and the training loss also fails to converge. On representative CSR tasks such as BoolQ, this instability leads to a clear degradation in dev performance compared with the full TS-PEFT variant (see Appendix A.2 for detailed curves and numerical results). These observations indicate that adaptive momentum estimation is essential for stabilizing the threshold update process in practice.

Module-wise Sparsity Distribution. In LLaMA3.1-8B, there are 32 layers in total. We compute the sparsity of q_proj, k_proj, and v_proj in each layer and take their average to obtain the sparsity distribution of TS-PEFT across modules (detailed results are provided in Appendix A.3). Overall, the sparsity of TS-LoRA and TS-AdaLoRA is relatively evenly distributed across layers, with standard deviations of 9.8 and 11.4, respectively. In contrast, TS-DoRA exhibits a much higher standard deviation of 41.3, showing a more “polarized” pattern. It should be noted that LoRA and AdaLoRA

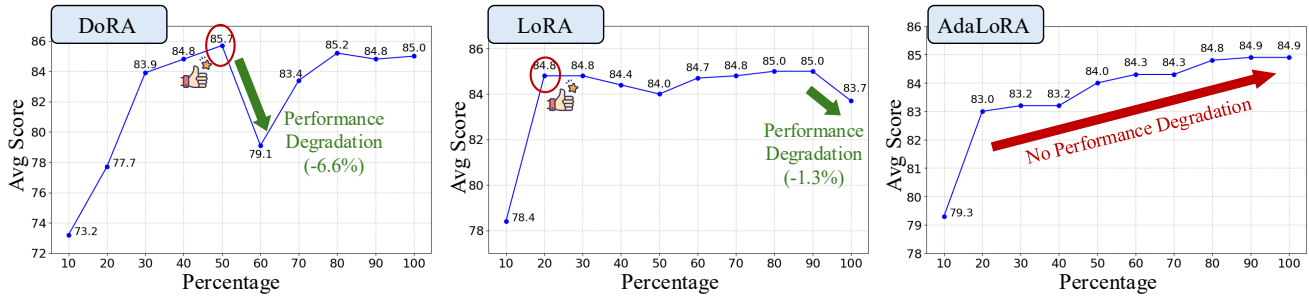


Figure 2: Performance of LLaMA3.1-8B on CSR benchmarks as the percentage of selected modules varies for each PEFT method.

	PIQA	BoolQ	HellaSwag	WinoGrande	SIQA	OBQA	ARC-e	ARC-c	Avg
S_low_50%	88.6	75.7	95.4	86.9	80.6	87.6	90.8	79.7	85.7
S_high_50%	88.2	62.2	92.2	85.2	80.2	86.2	90.4	79.9	83.0
norm_relative_50%	88.4	62.2	95.4	85.0	80.5	83.6	90.1	80.2	83.2
norm_abs_50%	88.4	52.7	85.8	83.9	78.7	86.2	89.6	79.0	80.5
random_50%	88.3	73.4	91.2	85.6	80.6	85.7	89.6	78.9	84.2
half_rank_50%	88.1	75.4	95.2	86.3	81.2	85.2	89.6	78.7	84.9

Table 4: The performance of LLaMA3.1-8B on the commonsense reasoning task using various selection methods.

share the same weight structure despite having different rank allocation strategies, whereas DoRA adopts a distinct parameterization by decomposing weights into magnitude and direction. We hypothesize that this structural difference leads to the stronger selectivity observed in TS-DoRA at the module level, naturally raising the question: are the modules with lower sparsity more critical for downstream tasks?

Token-level Sparsity as a Module Importance Indicator. To examine whether token-level sparsity can be used to identify important modules, we design a set of selection experiments based on the sparsity patterns learned by TS-DoRA. After completing TS-DoRA fine-tuning, we rank all modules by their average token sparsity and construct two main settings under the same parameter budget: (1) S_low_50%, which fine-tunes only the 50% of modules with the lowest sparsity, and (2) S_high_50%, which fine-tunes only the 50% of modules with the highest sparsity.

We compare these sparsity-based selections against several alternatives: norm_relative_50% (selecting the 50% of modules with the largest average $\|M(x_i)\|_2/\|W_0 x_i\|_2$), norm_abs_50% (the 50% with the largest average $\|M(x_i)\|_2$), random_50% (randomly selecting 50% of modules, averaged over three runs), and half_rank_50% (using all modules but halving the rank so that the total number of trainable parameters matches the 50% settings). The results in Table 4 show that S_low_50% not only significantly outperforms S_high_50% under the same parameter budget, but even surpasses fine-tuning all DoRA modules (whose mean score is 85.0). In contrast, norm-based selections, random choices, and half-rank full-module tuning all yield clearly inferior performance. This indicates that, in our setting, the token-level sparsity patterns learned by TS-DoRA provide a more reliable signal of module importance than simple norm statistics or random selection.

Effect of the Number of Target Modules. After using spar-

sity as the criterion for module importance ranking, we further examine the effect of varying the proportion of target modules while keeping the ranking fixed: we select different percentages of modules in ascending order of sparsity and fine-tune them. The results are shown in Figure 2. For AdaLoRA, performance remains largely unaffected as the proportion of target modules increases. However, for the others, “more is better” does not hold: DoRA achieves its best performance when using only 50% of the modules, LoRA reaches its optimal performance at 80%, and even using only 20% of the modules yields results close to the optimum.

In addition, LoRA and DoRA exhibit clear performance cliffs at certain points: for DoRA, performance drops by about 6.6% when increasing the target module proportion from 50% to 60%; for LoRA, increasing the proportion from 90% to 100% results in a drop of about 1.3%. This phenomenon indicates that jointly training modules with higher sparsity may negatively interfere with overall performance. In contrast, AdaLoRA is less sensitive to such “low-importance modules,” as its dynamic rank allocation redistributes capacity across modules.

5 Conclusion

This paper revisits parameter-efficient fine-tuning from a token-level perspective and shows that standard PEFT methods exhibit substantial redundancy by uniformly updating all token positions within selected layers. We propose TS-PEFT, which introduces a learnable threshold gate to selectively apply PEFT updates to only about 40–60% of token positions, yet consistently matches or surpasses strong baselines. Our analyses further show that the resulting token-level sparsity patterns provide a meaningful signal of module importance, enabling more effective module selection under the same parameter budget and offering a basis for future work on more efficient sparse fine-tuning and inference.

References

[Chen *et al.*, 2024] Shaoxiang Chen, Zequn Jie, and Lin Ma. Llava-mole: Sparse mixture of lora experts for mitigating data conflicts in instruction finetuning mllms. *arXiv preprint arXiv:2401.16160*, 2024.

[Croitoru *et al.*, 2023] Florinel-Alin Croitoru, Vlad Hondru, Radu Tudor Ionescu, and Mubarak Shah. Diffusion models in vision: A survey. *IEEE transactions on pattern analysis and machine intelligence*, 45(9):10850–10869, 2023.

[Dubey *et al.*, 2024] Abhimanyu Dubey, Abhinav Jauhri, Abhinav Pandey, Abhishek Kadian, Ahmad Al-Dahle, Aiesha Letman, Akhil Mathur, Alan Schelten, Amy Yang, Angela Fan, et al. The llama 3 herd of models. *arXiv e-prints*, pages arXiv-2407, 2024.

[Fedus *et al.*, 2022] William Fedus, Barret Zoph, and Noam Shazeer. Switch transformers: Scaling to trillion parameter models with simple and efficient sparsity. *Journal of Machine Learning Research*, 23(120):1–39, 2022.

[Han *et al.*, 2024] Zeyu Han, Chao Gao, Jinyang Liu, Jeff Zhang, and Sai Qian Zhang. Parameter-efficient fine-tuning for large models: A comprehensive survey. *Transactions on Machine Learning Research*, 2024.

[He *et al.*, 2021] Pengcheng He, Jianfeng Gao, and Weizhu Chen. Debertav3: Improving deberta using electra-style pre-training with gradient-disentangled embedding sharing. In *International Conference on Learning Representations*, 2021.

[Hu *et al.*, 2022] Edward J Hu, Yelong Shen, Phillip Wallis, Zeyuan Allen-Zhu, Yuanzhi Li, Shean Wang, Lu Wang, Weizhu Chen, et al. Lora: Low-rank adaptation of large language models. *International Conference on Learning Representations*, 1(2):3, 2022.

[Hu *et al.*, 2023] Zhiqiang Hu, Lei Wang, Yihuai Lan, Wanyu Xu, Ee-Peng Lim, Lidong Bing, Xing Xu, Soujanya Poria, and Roy Lee. Llm-adapters: An adapter family for parameter-efficient fine-tuning of large language models. In *Proceedings of the 2023 conference on empirical methods in natural language processing*, pages 5254–5276, 2023.

[Jiang *et al.*, 2024] Albert Q Jiang, Alexandre Sablayrolles, Antoine Roux, Arthur Mensch, Blanche Savary, Chris Bamford, Devendra Singh Chaplot, Diego de las Casas, Emma Bou Hanna, Florian Bressand, et al. Mixtral of experts. *arXiv preprint arXiv:2401.04088*, 2024.

[Kingma *et al.*, 2015] Diederik Kingma, Jimmy Ba Adam, et al. A method for stochastic optimization. In *International conference on learning representations (ICLR)*, volume 5. California;, 2015.

[Kopiczko *et al.*, 2024] Dawid Jan Kopiczko, Tijmen Blankevoort, and Yuki M Asano. Vera: Vector-based random matrix adaptation. In *International Conference on Learning Representations*, 2024.

[Lester *et al.*, 2021] Brian Lester, Rami Al-Rfou, and Noah Constant. The power of scale for parameter-efficient prompt tuning. In *Proceedings of the 2021 Conference on Empirical Methods in Natural Language Processing*, pages 3045–3059, 2021.

[Li and Liang, 2021] Xiang Lisa Li and Percy Liang. Prefix-tuning: Optimizing continuous prompts for generation. In *Proceedings of the 59th Annual Meeting of the Association for Computational Linguistics and the 11th International Joint Conference on Natural Language Processing (Volume 1: Long Papers)*, pages 4582–4597, 2021.

[Liu *et al.*, 2023] Haotian Liu, Chunyuan Li, Qingyang Wu, and Yong Jae Lee. Visual instruction tuning. *Advances in neural information processing systems*, 36:34892–34916, 2023.

[Liu *et al.*, 2024a] Haotian Liu, Chunyuan Li, Yuheng Li, and Yong Jae Lee. Improved baselines with visual instruction tuning. In *Proceedings of the IEEE/CVF conference on computer vision and pattern recognition*, pages 26296–26306, 2024.

[Liu *et al.*, 2024b] Qidong Liu, Xian Wu, Xiangyu Zhao, Yuanshao Zhu, Derong Xu, Feng Tian, and Yefeng Zheng. When moe meets llms: Parameter efficient fine-tuning for multi-task medical applications. In *Proceedings of the 47th International ACM SIGIR Conference on Research and Development in Information Retrieval*, pages 1104–1114, 2024.

[Liu *et al.*, 2024c] Shih-Yang Liu, Chien-Yi Wang, Hongxu Yin, Pavlo Molchanov, Yu-Chiang Frank Wang, Kwang-Ting Cheng, and Min-Hung Chen. Dora: Weight-decomposed low-rank adaptation. In *Forty-first International Conference on Machine Learning*, 2024.

[Liu *et al.*, 2024d] Yixin Liu, Kai Zhang, Yuan Li, Zhiling Yan, Chujie Gao, Ruoxi Chen, Zhengqing Yuan, Yue Huang, Hanchi Sun, Jianfeng Gao, et al. Sora: A review on background, technology, limitations, and opportunities of large vision models. *arXiv preprint arXiv:2402.17177*, 2024.

[Ma *et al.*, 2023] Xinyin Ma, Gongfan Fang, and Xinchao Wang. Llm-pruner: On the structural pruning of large language models. *Advances in neural information processing systems*, 36:21702–21720, 2023.

[Parikh *et al.*, 2014] Neal Parikh, Stephen Boyd, et al. Proximal algorithms. *Foundations and trends® in Optimization*, 1(3):127–239, 2014.

[Tan *et al.*, 2024] Zhen Tan, Tianlong Chen, Zhenyu Zhang, and Huan Liu. Sparsity-guided holistic explanation for llms with interpretable inference-time intervention. In *Proceedings of the AAAI conference on artificial intelligence*, volume 38, pages 21619–21627, 2024.

[Wang *et al.*, 2018] Alex Wang, Amanpreet Singh, Julian Michael, Felix Hill, Omer Levy, and Samuel Bowman. Glue: A multi-task benchmark and analysis platform for natural language understanding. In *Proceedings of the 2018 EMNLP workshop BlackboxNLP: Analyzing and interpreting neural networks for NLP*, pages 353–355, 2018.

[Xia *et al.*, 2024] Mengzhou Xia, Tianyu Gao, Zhiyuan Zeng, and Danqi Chen. Sheared LLaMA: Accelerating language model pre-training via structured pruning.

In *International Conference on Learning Representations*, 2024.

[Xu *et al.*, 2024] Peng Xu, Wenqi Shao, Mengzhao Chen, Shitao Tang, Kaipeng Zhang, Peng Gao, Fengwei An, Yu Qiao, and Ping Luo. Besa: Pruning large language models with blockwise parameter-efficient sparsity allocation. In *International Conference on Learning Representations*, 2024.

[Yao *et al.*, 2024] Yifan Yao, Jinhao Duan, Kaidi Xu, Yuanfang Cai, Zhibo Sun, and Yue Zhang. A survey on large language model (llm) security and privacy: The good, the bad, and the ugly. *High-Confidence Computing*, 4(2):100211, 2024.

[Zadouri *et al.*, 2024] Ted Zadouri, Ahmet Üstün, Arash Ahmadian, Beyza Ermis, Acyr Locatelli, and Sara Hooker. Pushing mixture of experts to the limit: Extremely parameter efficient moe for instruction tuning. In *International Conference on Learning Representations*, 2024.

[Zhang *et al.*, 2023] Qingru Zhang, Minshuo Chen, Alexander Bukharin, Pengcheng He, Yu Cheng, Weizhu Chen, and Tuo Zhao. Adaptive budget allocation for parameter-efficient fine-tuning. In *International Conference on Learning Representations*. Openreview, 2023.

A Appendix

A.1 LLM Usage Statement

During the preparation of this manuscript, the authors utilized a large language model (LLM) exclusively for grammar and language polishing. All technical content, scientific claims, and experimental results were conceived, derived, and verified solely by the authors.

A.2 The training loss progression with and without the Adaptive Moment Estimation

Figure 3 illustrates the training dynamics of a single TS-PEFT layer (the `v_proj` in `layers.20.self_attn` of LLaMA3.1-8B) with and without Adam-style momentum on the threshold τ . In both subfigures, the blue curve shows the training loss, while the red dashed curve tracks the corresponding threshold value over training steps (right-hand axis). When momentum is enabled (Figure 3(a)), the threshold increases smoothly and gradually saturates around a stable value, while the loss decreases rapidly at the beginning and then oscillates mildly around a low level. This indicates that τ can adapt to the task in a stable manner without causing large fluctuations in the optimization trajectory.

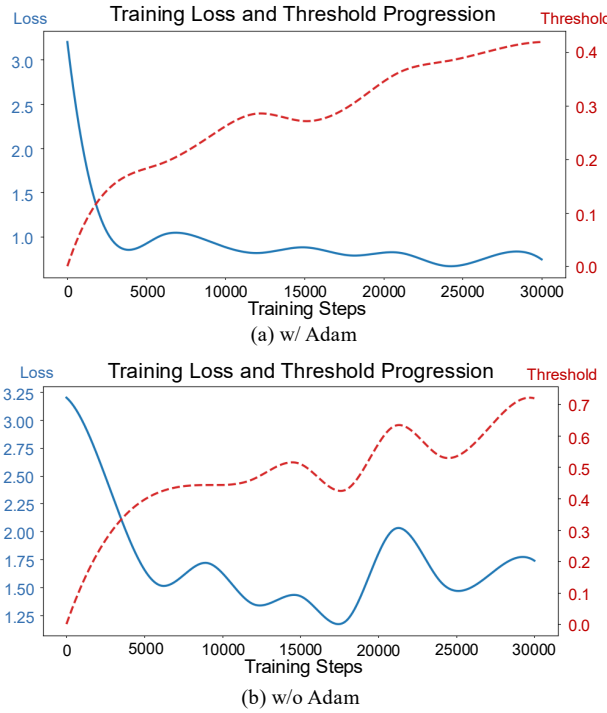


Figure 3: Training loss progression for layer `base_model.layers.20.self_attn.v_proj` of LLaMA3.1-8B.

In contrast, when we remove the adaptive moment estimation and update τ using plain gradient descent (Figure 3(b)), the threshold trajectory becomes highly oscillatory and eventually drifts to a much larger range (above 0.6). The loss curve also exhibits large, persistent oscillations and fails to converge to a similarly low level as in Figure 3(a). This unstable behavior at the layer level is consistent with the

degradation observed on downstream CSR benchmarks such as BoolQ: the dev accuracy drops noticeably compared with the full TS-PEFT variant that uses Adam-style updates for τ . These results provide direct empirical evidence that adaptive momentum estimation is crucial for stabilizing the learning of token-level thresholds in practice.

A.3 Module-wise average sparsity of LLaMA3.1-8B on the commonsense reasoning task

Table 5 reports the detailed module-wise sparsity of TS-LoRA, TS-DoRA, and TS-AdaLoRA on LLaMA3.1-8B for commonsense reasoning. For each transformer layer (indexed from 0 to 31), we measure the token-level sparsity of the PEFT updates in the query, key, and value projections (`q_proj`, `k_proj`, and `v_proj`), and then compute their average (“avg” column). The last row summarizes the mean sparsity over all layers for each method. A dash (“–”) indicates that the corresponding module is not assigned any rank (i.e., effectively pruned by the underlying PEFT scheme).

From the table, we observe that TS-LoRA and TS-AdaLoRA exhibit relatively smooth sparsity profiles across layers: their per-layer averages mostly stay within the 50%–70% range, and no single layer dominates the overall sparsity pattern. This matches the moderate standard deviations reported in the main text (9.8 for TS-LoRA and 11.4 for TS-AdaLoRA), suggesting that these two methods tend to distribute token-level updates more evenly over depth. In contrast, TS-DoRA shows a much more polarized pattern: several layers (e.g., layers 0–2, 5–7, 11, 17, 24, 29) have near-100% sparsity in one or more projections, while a few layers (such as 8, 9, 14, 22) maintain comparatively low sparsity. This leads to a much larger standard deviation (41.3), indicating that TS-DoRA concentrates effective updates into a smaller subset of layers. These fine-grained statistics support our observation in the main paper that the token-level sparsity learned by TS-DoRA can serve as a strong indicator of module importance and motivates the subsequent experiments that select only the low-sparsity (high-importance) modules for fine-tuning.

A.4 Hyperparameters

Across all experiments, we tune the sparsity-related hyperparameters s and λ separately from the other training configurations. For CSR and VIT, we fix the scaling factor at $s = 4 \times 10^{-5}$ and select λ from the interval $[10^{-7}, 10^{-3}]$ based on development performance. For NLU tasks, we instead set $s = 1 \times 10^{-4}$ and choose λ from $[10^{-8}, 10^{-3}]$. The remaining hyperparameters, including rank, scaling coefficient, dropout rate, optimizer, learning rate, scheduler, batch size, number of epochs, and target modules, are summarized in Table 6.

Layer	TS-LoRA				TS-DoRA				TS-AdaLoRA			
	q-proj	k-proj	v-proj	avg	q-proj	k-proj	v-proj	avg	q-proj	k-proj	v-proj	avg
0	65.6	77.6	0.0	47.7	100.0	0.0	0.0	33.3	-	-	76.9	76.9
1	59.7	65.5	54.8	60.0	100.0	0.0	65.0	55.0	62.3	84.5	68.4	71.8
2	62.8	64.9	51.5	59.7	100.0	100.0	57.2	85.7	57.3	75.0	81.7	71.3
3	60.1	64.4	56.3	60.2	99.8	100.0	37.1	79.0	67.6	68.7	81.9	72.7
4	63.7	67.6	56.6	62.6	24.6	0.0	83.0	35.9	48.2	70.2	75.8	64.7
5	57.9	62.6	54.8	58.4	0.0	0.0	30.9	10.3	49.6	86.4	80.9	72.3
6	62.4	60.6	48.4	57.1	100.0	0.0	62.9	54.3	70.7	84.8	66.1	73.9
7	61.3	65.9	51.2	59.5	0.0	0.0	82.8	27.6	59.8	86.6	77.2	74.5
8	60.8	65.8	50.4	59.0	70.5	57.1	60.2	62.6	54.0	93.6	60.7	69.4
9	65.9	51.1	53.1	56.7	0.0	11.6	47.4	19.7	52.0	72.4	61.2	61.9
10	57.7	58.7	52.8	56.4	0.0	0.0	41.3	13.8	51.3	82.5	64.2	66.0
11	58.5	57.5	42.3	52.8	91.7	77.2	76.1	81.7	54.2	86.6	65.0	68.6
12	51.9	68.2	49.9	56.7	0.0	0.0	2.1	0.7	50.7	87.9	56.0	64.9
13	58.9	68.3	51.2	59.5	90.2	90.0	35.1	71.7	61.3	73.4	56.1	63.6
14	57.1	60.6	48.9	55.6	0.0	82.6	44.6	42.4	62.0	68.6	44.8	58.5
15	63.2	63.5	51.0	59.3	81.2	0.0	35.2	38.8	66.3	69.0	46.0	60.4
16	58.5	69.9	55.9	61.4	99.8	100.0	3.6	67.8	59.2	86.9	48.8	65.0
17	62.9	70.8	54.7	62.8	99.3	100.0	30.9	76.7	61.6	74.0	53.6	63.1
18	67.3	75.9	61.3	68.2	99.5	70.0	47.0	72.2	62.6	94.7	62.5	73.3
19	65.6	64.4	54.0	61.3	98.0	0.0	78.5	58.8	66.9	80.5	62.7	70.0
20	67.8	66.0	47.5	60.4	97.6	0.0	0.8	32.8	65.5	85.8	54.7	68.6
21	58.2	63.5	44.2	55.3	99.4	100.0	42.4	80.6	61.0	69.1	45.4	58.5
22	62.8	57.6	58.2	59.5	99.8	98.0	79.5	92.4	64.5	70.8	59.7	65.0
23	70.0	71.7	55.6	65.8	99.5	2.5	14.0	38.7	69.6	71.9	57.7	66.4
24	72.3	63.0	53.5	62.9	0.0	0.3	46.0	15.4	68.8	73.7	67.2	69.9
25	69.8	63.2	56.3	63.1	0.2	0.0	4.7	1.6	58.6	65.8	76.9	67.1
26	65.1	70.2	56.4	63.9	9.4	94.2	56.5	53.4	64.4	74.5	67.7	68.8
27	68.9	67.2	68.2	68.1	99.8	95.1	45.1	80.0	62.7	85.8	78.3	75.6
28	57.8	58.9	61.5	59.4	17.9	99.9	94.9	70.9	63.8	76.2	86.1	75.4
29	71.6	78.7	49.3	66.5	0.0	100.0	11.4	37.1	63.9	74.4	79.7	72.7
30	59.5	59.6	57.2	58.8	0.0	100.0	39.2	46.4	67.8	68.6	72.9	69.8
31	64.4	67.3	46.1	59.3	100.0	0.0	1.2	33.7	69.3	71.0	57.7	66.0
avg	64.8	67.4	53.3	—	60.6	47.7	43.8	—	61.2	77.9	67.6	—

Table 5: Module-wise average sparsity (%) of LLaMA3.1-8B on commonsense reasoning. “-” denotes rank 0.

Task	Data	Rank	Scale	Dropout	Optimizer	LR	Scheduler	Batch	Epochs	Target
CSR	ALL	32	0.5	0.05	AdamW	1e-4	Linear	16	3	Q,K,V,Up,Down
VIT	ALL	128	0.5	0.05	AdamW	2e-4	Cosine	16	1	Q,K,V,O,Up,Down,Gate
NLU	CoLA	4	0.5	0.1	AdamW	4e-4	Linear	32	40	Q,K,V,O,I
NLU	MNLI	4	0.5	0.15	AdamW	2.5e-4	Linear	32	10	Q,K,V,O,I
NLU	QNLI	4	0.5	0.1	AdamW	2e-4	Linear	32	10	Q,K,V,O,I
NLU	RTE	4	0.5	0.2	AdamW	1e-4	Linear	32	80	Q,K,V,O,I
NLU	MRPC	4	0.5	0	AdamW	1e-4	Linear	32	60	Q,K,V,O,I
NLU	QQP	4	0.5	0.15	AdamW	4e-4	Linear	32	10	Q,K,V,O,I
NLU	SST-2	4	0.5	0	AdamW	4e-4	Linear	32	48	Q,K,V,O,I
NLU	STS-B	4	0.5	0.2	AdamW	5e-4	Linear	32	45	Q,K,V,O,I

Table 6: Hyperparameter configuration for our experiments.